

Article

Experimental Study of Temperature Effect on Methane Adsorption Dynamic and Isotherm

Yongchun Zhang ^{1,2}, Aiguo Hu ^{1,2}, Pei Xiong ², Hao Zhang ^{1,*} and Zhonghua Liu ^{3,*} 

¹ College of Energy Resource, Chengdu University of Technology, Chengdu 610059, China; hbjzyc@126.com (Y.Z.); huaiguo19842004@163.com (A.H.)

² Research Institute of Engineering and Technique, Sinopec Huabei Sub-Company, Zhengzhou 450006, China; xiongpei_2004@126.com

³ School of Petroleum and Natural Gas Engineering, Chongqing University of Science and Technology, Chongqing 401331, China

* Correspondence: zhanghao@cdut.edu.cn (H.Z.); liuzhonghua@cqust.edu.cn (Z.L.)

Abstract: Knowing the methane adsorption dynamic is of great importance for evaluating shale gas reserves and predicting gas well production. Many experiments have been carried out to explore the influence of many aspects on the adsorption dynamic of methane on shale rock. However, the temperature effect on the adsorption dynamic as a potential enhanced shale gas recovery has not been well addressed in the publications. To explore the temperature effect on the adsorption dynamic of methane on gas shale rock, we conducted experimental measurement by using the volumetric method. We characterized the adsorption dynamic of methane on gas shale powders and found that the curves of pressure response at different pressure steps and temperatures all have the same tendency to decrease fast at first, then slowly in the middle and remain stable at last, indicating the methane molecules are mainly adsorbed in the initial stage. Methane adsorption dynamic and isotherm can be well fitted by the Bangham model and the Freundlich model, respectively. The constant z of the Bangham model first decreases and then increases with equilibrium pressure increasing at each temperature, and it decreases with temperature increasing at the same pressure. The adsorption rate, constant k of the Bangham model, is linearly positively correlated with the natural log of the equilibrium pressure, and it decreases with temperature increasing at the same pressure. Constant K and n of the Freundlich model all decrease with temperature increasing, indicating that low temperatures are favorable for methane adsorption on shale powders, and high temperatures can obviously reduce constant K and n of the Freundlich model. Finally, we calculated isosteric enthalpy and found that isosteric enthalpy is linearly positively correlated with the adsorption amount. These results will be profoundly meaningful for understanding the mechanism of methane adsorption dynamic on shale powders and provide a potential pathway to enhance shale gas recovery.

Keywords: adsorption dynamic; Longmaxi shale; Bangham model; Freundlich model; adsorption isotherm; isostatic enthalpy



Citation: Zhang, Y.; Hu, A.; Xiong, P.; Zhang, H.; Liu, Z. Experimental Study of Temperature Effect on Methane Adsorption Dynamic and Isotherm. *Energies* **2022**, *15*, 5047. <https://doi.org/10.3390/en15145047>

Academic Editor: Daoyi Zhu

Received: 6 June 2022

Accepted: 4 July 2022

Published: 11 July 2022

Publisher's Note: MDPI stays neutral with regard to jurisdictional claims in published maps and institutional affiliations.



Copyright: © 2022 by the authors. Licensee MDPI, Basel, Switzerland. This article is an open access article distributed under the terms and conditions of the Creative Commons Attribution (CC BY) license (<https://creativecommons.org/licenses/by/4.0/>).

1. Introduction

Shale gas, as one of the most promising unconventional natural gas resources, has attracted increasing attention in recent years. As we know, adsorbed gas is a major type of shale gas stored in shale gas reservoir [1,2], which distributes from 20% to 85% of the total gas in shale gas reservoirs [3,4]. Therefore, characterizing the adsorption dynamic and knowing the temperature influence is of great significance for exploring the methane adsorption mechanism on gas shale.

In recent years, the experiments of methane adsorption dynamic have been conducted in many publications by using volumetric and gravimetric methods [5–7]. Gas-in-place evaluation can be accurately calculated based on the experimental measurements from laboratory [8]. Many scholars have pointed out that the methane adsorption on the gas

shale is closely correlated with kerogen types [9], TOC [10], mineral constituents of shale rock [11], pore structure [12,13], temperature [14] and moisture [15]. At the same time, the characteristics of methane adsorption and desorption are always revealed by fitting adsorption or desorption equations, such as the Langmuir model [16], Freundlich model [17,18] and modified Dubinin–Radushkevich model [19].

Meanwhile, methane adsorption dynamics have attracted attention from many scholars [1,20–22]. Yuan et al. [23] investigated the pore structure characteristics of Lower Silurian shale and the diffusion behavior of methane molecules, as well as the shale sample size influence on the adsorption and diffusion of methane. Chen et al. [24] studied the mechanisms of methane adsorption in terms of methane adsorption thermodynamics under the condition of high pressure. Rani et al. [25] characterized the adsorption dynamic of methane according to the unipore model and the modified unipore model, respectively. Dasani et al. [8] pointed out the adsorption dynamic of methane mixed with ethane in gas shale samples. Yang et al. [26] published a dynamic adsorption–diffusion equation after dynamic adsorption measurements under the certain condition of a constant pressure and then compared with the instantaneous adsorption–diffusion equation and diffusion equations. However, the adsorption dynamic of methane on Longmaxi gas shale is not still well characterized, and the temperature influence on the methane adsorption dynamic is also not clear.

In this study, for better understanding the temperature effect on methane adsorption dynamic, we conducted the experimental measurements of adsorption dynamic by using the volumetric method at different temperatures, as well as characterizing the adsorption dynamic for methane on gas shale powders and fitting the experimental data by using the Bangham model and the Freundlich model. Finally, we explored the temperature effect on the adsorption dynamic equation, isotherm equation and adsorption thermodynamics. These results are profoundly meaningful for advancing the mechanism of shale gas adsorption dynamic in shale reservoirs.

2. Experimental Design

2.1. Shale Samples

The shale samples from the lower of Silurian Longmaxi formation in northeast of Chongqing were crushed and then went through sieves with diameters of 0.25 and 0.125 mm in sequence. The shale powders between 0.25 and 0.125 mm in diameter were dried in an oven at a constant temperature of 60 °C, but some water may still have been trapped in the pores of shale samples. An amount of 130 g of gas shale powders was prepared for methane adsorption dynamic test. The density of shale samples was 2.56 g/cm³. Based on the experimental results of low-pressure nitrogen adsorption/desorption, the specific surface area was 26.58 m²/g, and the pore sizes of the shale sample were mainly distributed in the broad mesoporous region. According to X-ray diffraction, the shale samples mainly contained quartz, clay mineral, dolomite and plagioclase, and their contents were 46.2%, 32.3%, 9.9% and 5.1%, respectively.

2.2. Experimental Apparatus

An experimental apparatus is shown in Figure 1 to test the pressure response during the dynamic process of methane adsorption on shale powders, which was designed using the volumetric method and consisted of many parts, such as methane tank, nitrogen tank, gas compressor, vacuum pump, pressure transducers, reference cell, sample cell, water bath, computer and other valves. The potentiometric pressure transducers were used in this work, and their maximum pressure was 40 MPa, and the precision was 0.25% of the full-scale value. The water bath could work from an indoor temperature to 100 °C, and the control precision was achieved to 0.2 °C. Methane in the methane tank was used for the adsorption dynamic test on the shale powders, and nitrogen contained in the nitrogen tank was applied to check the leak of the experimental setup and obtain the void volume of shale powders loaded in the sample cell. To make the experimental temperature stable, a

water bath with a temperature controller was added. To read the pressure response during the experimental procedure, pressure transducers were used, and the data were recorded using a computer.

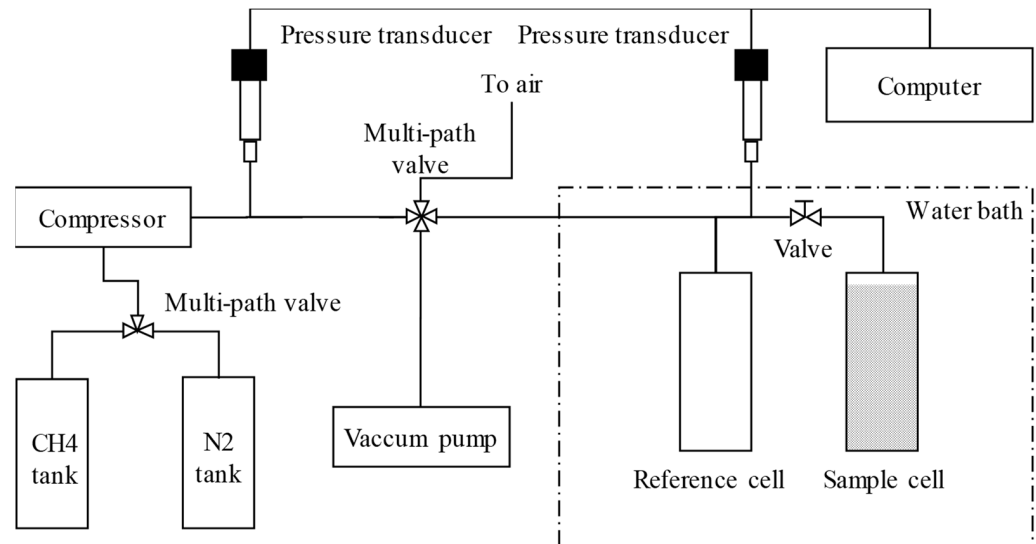


Figure 1. Schematic diagram of experimental apparatus.

2.3. Procedures

To characterize the adsorption dynamic of methane on gas shale, the procedures were shown as follows:

1. Preparation. An amount of 130.00 g of shale powders, whose diameter was between 0.125 and 0.25 mm, was loaded into the sample cell and then heated and maintained at 30, 40 or 50 °C, respectively.
2. Leak check of experimental apparatus. To check the leak of the apparatus at a certain pressure and temperature, nitrogen was used until the pressure reached and maintained stability for two hours, and the temperature remained stable.
3. Free volume determination. Free volume is defined as the space between the shale powders and within the powders and was calculated according to Boyle's law by using the different equilibrium pressures.
4. Apparatus vacuum. The apparatus was vacuumed down to 10^{-5} Pa for 24 h to completely remove the gas molecules from the shale powders.
5. Adsorption dynamic determination. After the pressure of the reference cell full of pure methane remained stable, the reference cell and sample cell were connected by opening the valve between them. Then, the two stable pressures before and after the methane expansion were read and recorded. This procedure should be repeated until an equilibrium pressure of about 30 MPa is reached. The pressure response during the dynamic process of methane adsorption was read and recorded.

3. Mathematical Model

3.1. Dynamic Model

The Bangham model is widely used for modeling methane adsorption dynamic, and it is expressed as the following equation [24,27–29]:

$$q_t = q_e \left(1 - e^{-kt^z}\right) \quad (1)$$

where z is a constant, and k is the adsorption rate of the Bangham equation.

Equation (1) can be shown as the following formula:

$$-\ln \frac{q_e - q_t}{q_e} = kt^z \quad (2)$$

The linear formula of the Bangham equation can be shown as follows:

$$\ln\left(-\ln \frac{q_e - q_t}{q_e}\right) = \ln(k) + z\ln(t) \quad (3)$$

From Equation (3), the relationship between $\ln\left(-\ln \frac{q_e - q_t}{q_e}\right)$ and $\ln(t)$ should be fitted into linear equation, and k and z can be obtained according to the y-intercept of $\ln(k)$ and the slope of z .

3.2. Isotherm Model

The Freundlich model is a classical isothermal adsorption model and regarded as an extension of the Henry model [30]. The equation can be expressed as follows:

$$V = KP^n \quad (4)$$

where V is the adsorption capacity per unit mass samples (cc/g), K is the Freundlich constant related to a measure of adsorption capacity (cc/g/MPa), and P is the equilibrium pressure (MPa). n is a constant, the strength of the adsorption. Some articles [31,32] used the following linear equation, which is rearranged from Equation (4):

$$\lg(V) = n \cdot \lg(P) + \lg(K) \quad (5)$$

Additionally, the log-log plot of V versus P should be a straight line with the slope of n and the y-intercept of $\lg(K)$.

3.3. Absolute Adsorption Amount

The adsorption amount through a measurement test can be defined as excess adsorption amount, and the absolute adsorption amount can be converted as the following equation [33]:

$$n_{abs} = \frac{n_{excess}}{1 - \rho_{gas}/\rho_{ads}} \quad (6)$$

where n_{abs} is the absolute amount of methane adsorption, cc/g; n_{excess} is the excess amount of methane adsorption, cc/g; ρ_{gas} is the density of free phase gas, g/cc; and ρ_{ads} is the density of adsorbed phase gas in g/cc, which is determined as the value of 0.527 g/cc [34] and used in this study.

4. Results and Discussion

4.1. Dynamic Characteristics of Methane Adsorption

Figures 2–4 show the plots of pressure response and adsorption versus time under different pressure step at 30, 40 or 50 °C, respectively. Obviously, it is shown that the pressure drops fast at first, then slowly in the middle and reaches and maintains stability at last. Meanwhile, the absolute amount of methane adsorption increases quickly initially, then slowly in the middle and reaches a constant at last. These two curves, which describe the adsorption dynamic of methane, have similar characteristics to the other studies [8,24], indicating that the methane molecules are mainly adsorbed in the initial stage.

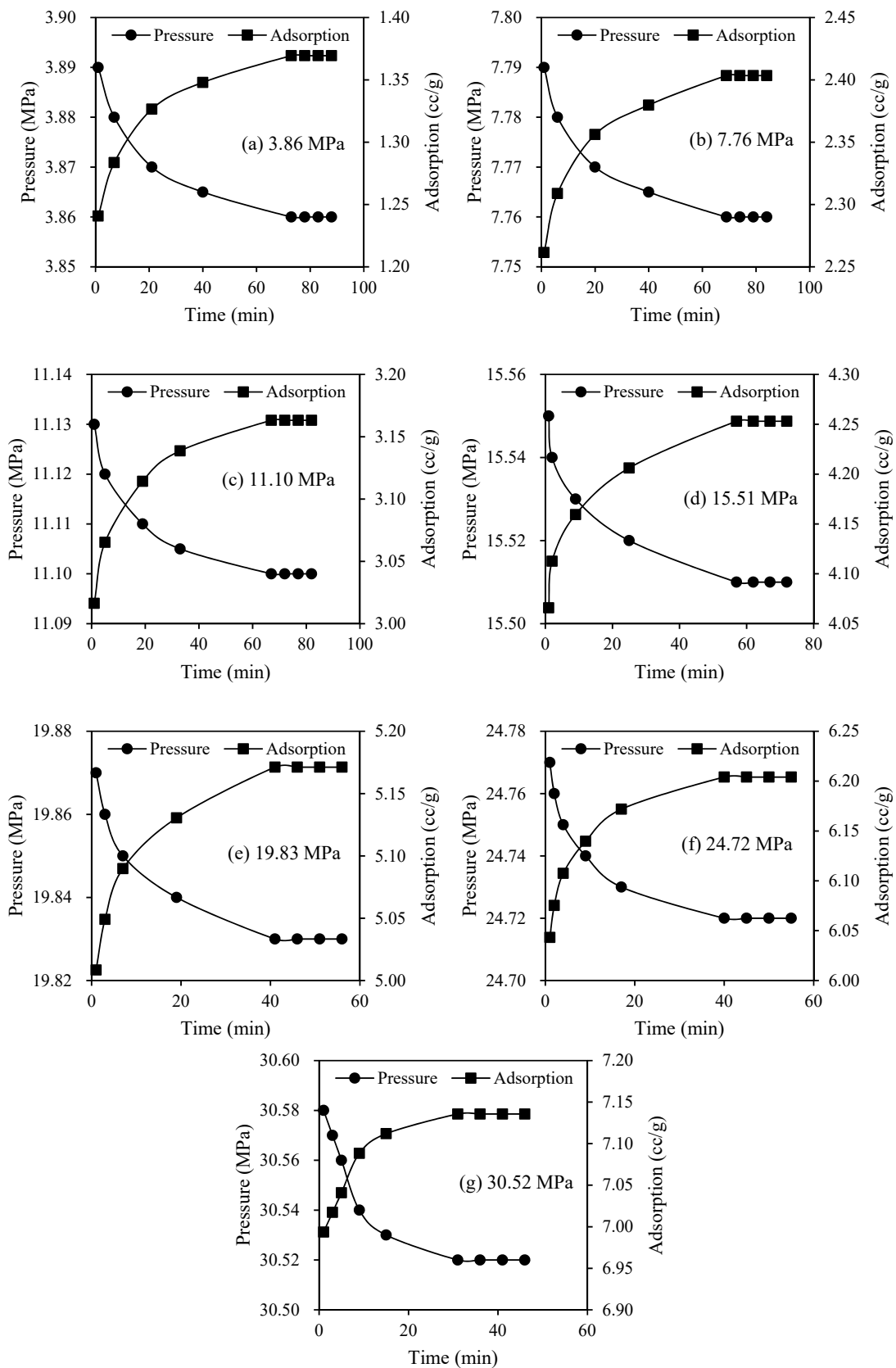


Figure 2. Methane adsorption dynamic on shale sample at seven pressure steps and 30 °C.

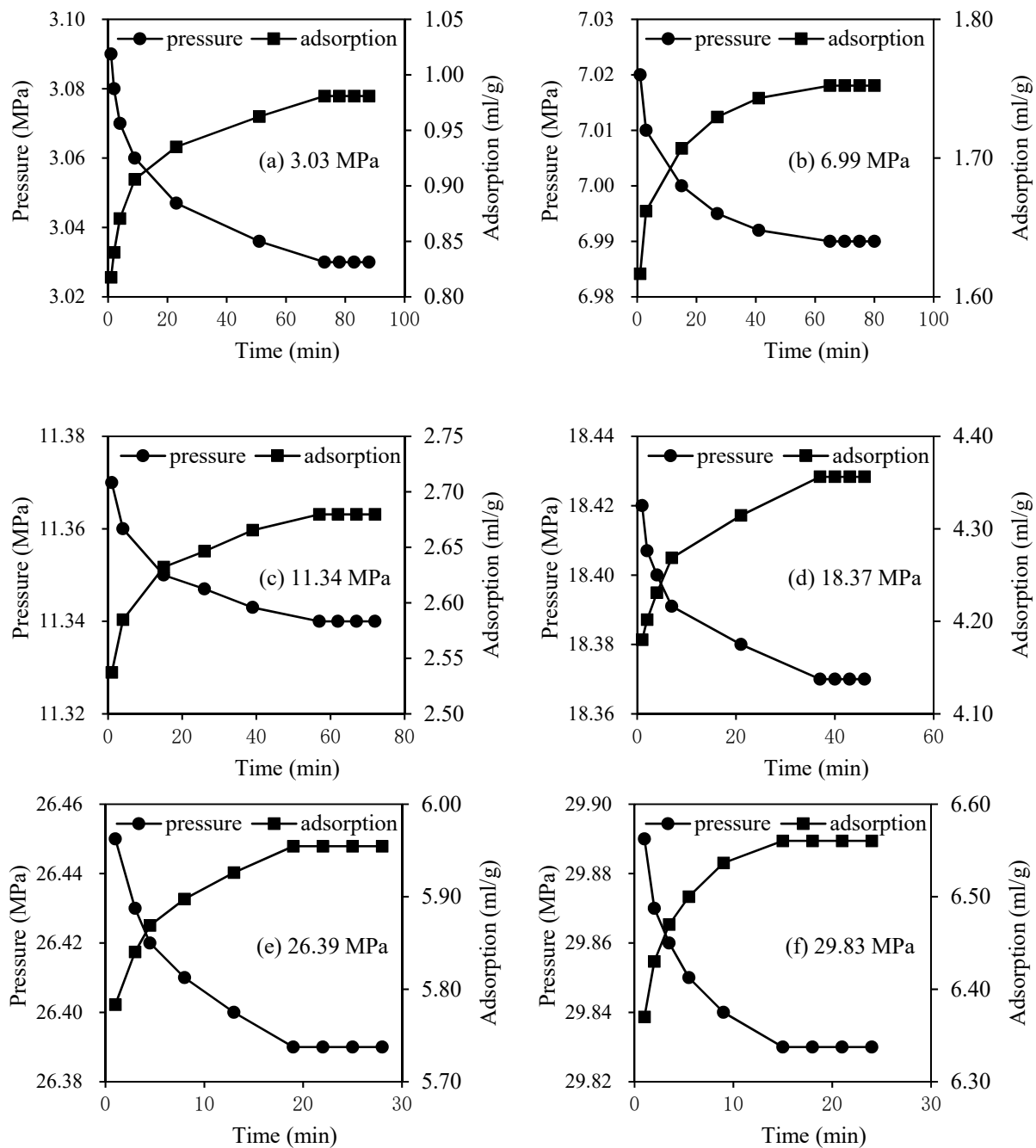


Figure 3. Methane adsorption dynamic on shale sample at six pressure steps and 40 °C.

To be more specific, at the beginning, most of the active surface sites are vacant and favorable for methane molecules adsorption on shale powders because the adsorption rate is positively correlated with the available vacancies [25]. Furthermore, at first, the high concentration driving force between the methane molecules spurs the mass free phase gas to the adsorbed phase gas. Additionally, in the middle, the repulsion of methane molecules gradually becomes the major force to determine the adsorption dynamic of methane molecules [35]. Therefore, the tendency of the adsorption dynamic curves demonstrates the synthetic influence of the high concentration driving force and repulsion of methane molecules on the adsorption dynamic of methane molecules.

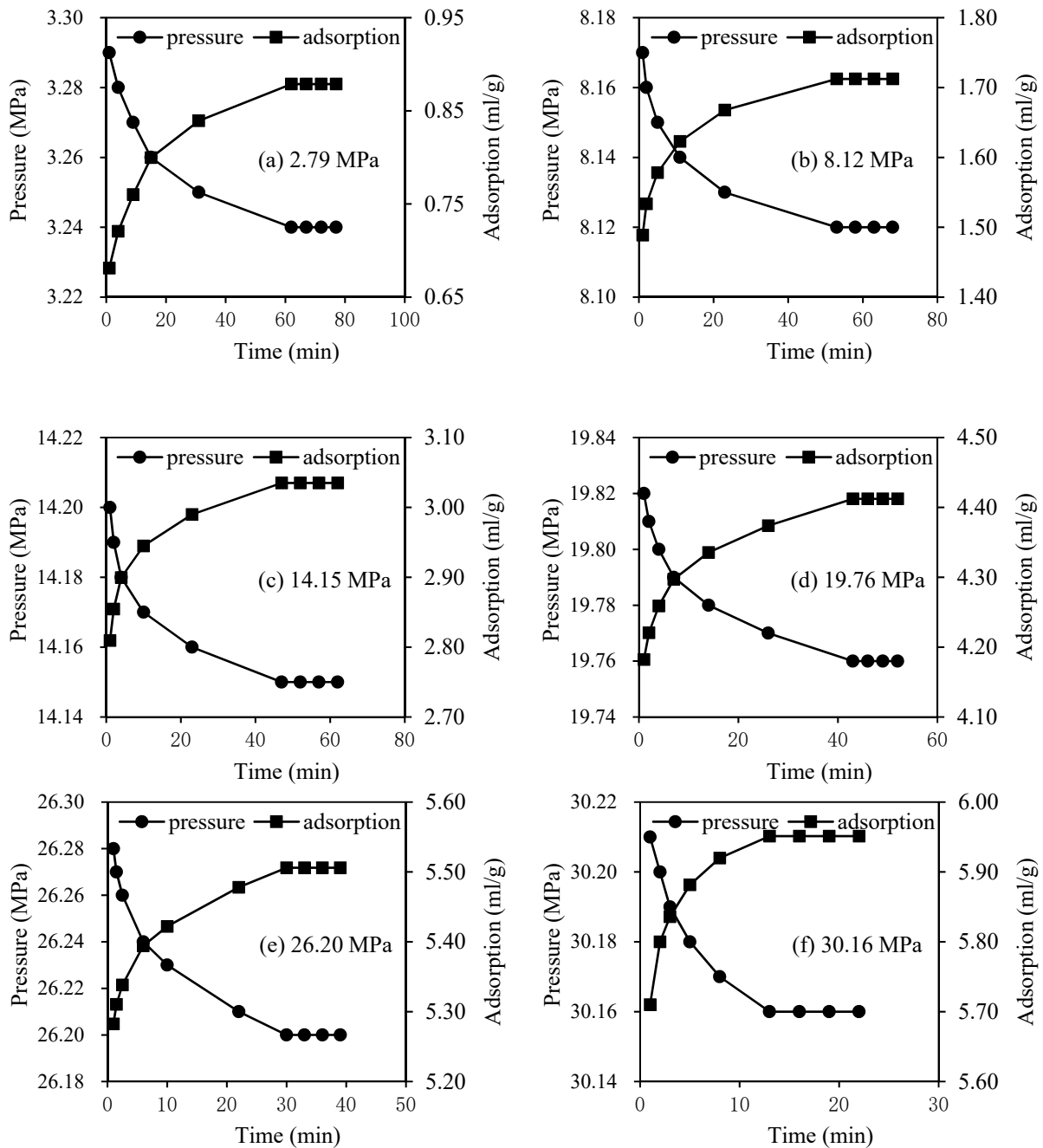


Figure 4. Methane adsorption dynamic on shale sample at six pressure steps and 50 °C.

4.2. Dynamic Model Fitting

Figure 5 shows the continuous change of $\ln(-\ln(\frac{q_e - q_t}{q_e}))$ versus $\ln(t)$ under seven pressure steps using Equation (3) based on the Bangham model at 30 °C. It is clearly shown that $\ln(-\ln(\frac{q_e - q_t}{q_e}))$ increases linearly with the increasing $\ln(t)$ because the correlation coefficients (R^2), respectively, are 0.9253, 0.9418, 0.9435, 0.9745, 0.9706, 0.9655 and 0.8585, as listed in Table 1, with the average of 0.9400. Therefore, q_t can be well fitted with t by using the Bangham model at each pressure step.

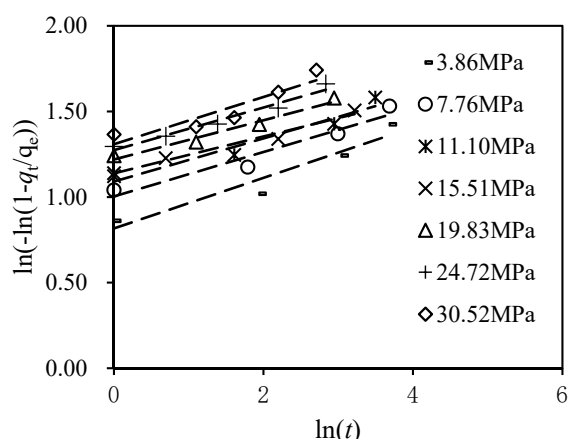


Figure 5. Fitting methane adsorption dynamic using Bangham model at 30 °C.

Table 1. The results of fitting methane adsorption dynamic using Bangham model at 30 °C.

NO	P (MPa)	Fitting Equation	R ²	Model	k	z
1	3.86	$y = 0.1475x + 0.8168$	0.9253	$q_t = 1.3694(1 - e^{-2.2632t^{0.1457}})$	2.2632	0.1457
2	7.76	$y = 0.1295x + 1.0038$	0.9418	$q_t = 2.4034(1 - e^{-2.7286t^{0.1295}})$	2.7286	0.1295
3	11.10	$y = 0.1259x + 1.0906$	0.9435	$q_t = 3.1632(1 - e^{-2.9761t^{0.1259}})$	2.9761	0.1259
4	15.51	$y = 0.1076x + 1.1385$	0.9745	$q_t = 4.2530(1 - e^{-3.1221t^{0.1076}})$	3.1221	0.1076
5	19.83	$y = 0.1145x + 1.2193$	0.9706	$q_t = 5.1712(1 - e^{-3.3848t^{0.1145}})$	3.3848	0.1145
6	24.72	$y = 0.1244x + 1.2742$	0.9655	$q_t = 6.2041(1 - e^{-3.5758t^{0.1244}})$	3.5758	0.1244
7	30.52	$y = 0.1379x + 1.3087$	0.8585	$q_t = 7.1357(1 - e^{-3.7014t^{0.1379}})$	3.7014	0.1379

The fitting equations, the Bangham model, the adsorption rate constant and the constant z are listed in Table 1. At different pressure steps, the adsorption rate constants are 2.2632, 2.7286, 2.9761, 3.1221, 3.3848, 3.5758 and 3.7014, respectively, indicating that the adsorption rate constant increases with the equilibrium pressure increasing. The constant z, respectively, is 0.1457, 0.1295, 0.1259, 0.1076, 0.1145, 0.1244 and 0.1379, revealing that z (a constant of the Bangham model) first decreases and then increases with the equilibrium pressure increasing.

Figure 6 shows the relationship between $\ln(-\ln(\frac{q_e - q_t}{q_e}))$ and $\ln(t)$ under six pressure steps by using Equation (3) at 40 °C. It can be seen that $\ln(-\ln(\frac{q_e - q_t}{q_e}))$ increases linearly with $\ln(t)$ increasing because the correlation coefficients at each pressure step, respectively, are 0.9938, 0.9430, 0.9411, 0.9600, 0.9512 and 0.9355, as listed in Table 2, with the average of 0.9541. Therefore, the Bangham model can be well fitted in the relationship between q_t and t for different pressure steps.

Table 2. The results of fitting methane adsorption dynamic using Bangham model at 40 °C.

NO	P (MPa)	Fitting Equation	R ²	Model	K	z
1	3.03	$y = 0.1993x + 0.5350$	0.9938	$q_t = 0.9809(1 - e^{-1.7074t^{0.1993}})$	1.7074	0.1993
2	6.99	$y = 0.1795x + 0.9028$	0.9430	$q_t = 1.7522(1 - e^{-2.4665t^{0.1795}})$	2.4665	0.1795
3	11.34	$y = 0.1469x + 1.0387$	0.9411	$q_t = 2.6797(1 - e^{-2.8255t^{0.1469}})$	2.8255	0.1469
4	18.37	$y = 0.1240x + 1.1319$	0.9600	$q_t = 4.3562(1 - e^{-3.1015t^{0.1240}})$	3.1015	0.1240
5	26.39	$y = 0.1544x + 1.2356$	0.9512	$q_t = 5.9546(1 - e^{-3.4404t^{0.1544}})$	3.4404	0.1544
6	29.83	$y = 0.2012x + 1.2358$	0.9355	$q_t = 6.5604(1 - e^{-3.4411t^{0.2012}})$	3.4411	0.2012

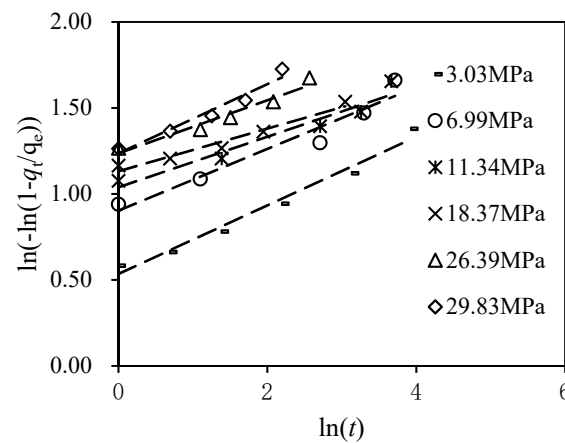


Figure 6. Fitting methane adsorption dynamic using Bangham model at 40 °C.

The fitting results, including the fitting equations, the Bangham model, the adsorption rate constant and the constant z are listed in Table 2. At six pressure steps, the adsorption rate constants are 1.7074, 2.4665, 2.8255, 3.1015, 3.4404 and 3.4411, respectively, indicating that k (adsorption rate constant) increases with the equilibrium pressure increasing. The constant z , respectively, is 0.1993, 0.1795, 0.1469, 0.1240, 0.1544 and 0.2012, revealing that z (a constant of the Bangham model) first decreases and then increases with the equilibrium pressure increasing.

Figure 7 shows the plots of $\ln(-\ln(\frac{q_e - q_t}{q_e}))$ and $\ln(t)$ under six pressure steps using Equation (3) at 50 °C. It is clearly shown that $\ln(-\ln(\frac{q_e - q_t}{q_e}))$ increases linearly with $\ln(t)$ increasing because the correlation coefficients at each pressure step, respectively, are 0.9170, 0.9743, 0.9864, 0.9610, 0.9411 and 0.9964, as listed in Table 3, with the average of 0.9627. Thus, q_t can be well fitted with t by using the Bangham model for six pressure steps.

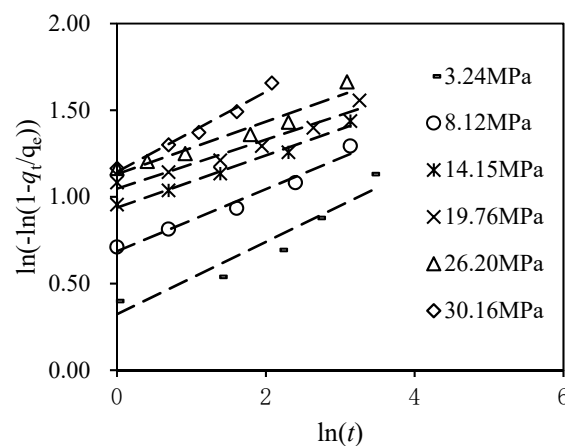


Figure 7. Fitting methane adsorption dynamic using Bangham model at 50 °C.

Table 3. The results of fitting methane adsorption dynamic using Bangham model at 50 °C.

NO	P(MPa)	Fitting Equation	R ²	Model	k	z
1	3.24	$y = 0.2086x + 0.3231$	0.9170	$q_t = 0.8787(1 - e^{-1.3814t^{0.2086}})$	1.3814	0.2086
2	8.12	$y = 0.1791x + 0.6864$	0.9743	$q_t = 1.7123(1 - e^{-1.9866t^{0.1791}})$	1.9866	0.1791
3	14.15	$y = 0.1508x + 0.9378$	0.9864	$q_t = 3.035(1 - e^{-2.5544t^{0.1508}})$	2.5544	0.1508
4	19.76	$y = 0.1415x + 1.0473$	0.9610	$q_t = 4.4132(1 - e^{-2.8499t^{0.1415}})$	2.8499	0.1415
5	26.20	$y = 0.1514x + 1.1314$	0.9411	$q_t = 5.206(1 - e^{-3.1000t^{0.1514}})$	3.1000	0.1514
6	30.16	$y = 0.1932x + 1.1660$	0.9964	$q_t = 5.9513(1 - e^{-3.2091t^{0.1932}})$	3.2091	0.1932

Table 3 lists the fitting results, including the fitting equations, the Bangham model, the adsorption rate constant and the constant z . K (adsorption rate constant) at six pressure steps, respectively, is 1.3814, 1.9866, 2.5544, 2.8499, 3.1000 and 3.2091, indicating that k increases with the equilibrium pressure increasing. The constant z (a constant of the Bangham model), respectively, is 0.2086, 0.1791, 0.1508, 0.1415, 0.1514 and 0.1932, revealing that z first decreases and then increases with the equilibrium pressure increasing.

4.3. Effect of Temperature on Constant z

To investigate the temperature influence on the adsorption dynamic of methane on shale powders, the constant z of the Bangham model at 30, 40 and 50 °C is plotted versus the equilibrium pressure, as shown in Figure 8. Obviously, it is shown that the curves of the constant z at different temperature conditions have a similar tendency to decrease first and then increase with the equilibrium pressure increasing. Furthermore, at the same pressure point, the higher the temperature, the smaller the constant z , indicating that temperature can obviously reduce the constant z . Therefore, the constant z first decreases and then increases with the equilibrium pressure increasing at each temperature, and it decreases with the temperature increasing at the same pressure.

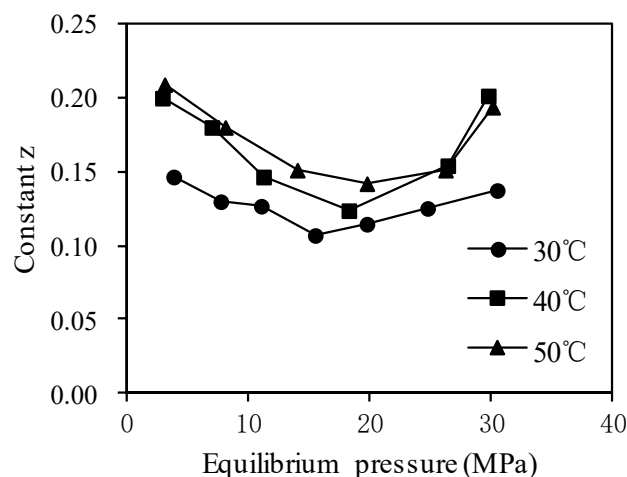


Figure 8. Constant Z versus equilibrium pressure at different temperature.

4.4. Effect of Temperature on Adsorption Rate Constant

The plot of the adsorption rate constant versus equilibrium pressure at 30, 40 and 50 °C is shown in Figure 9 to illustrate the temperature effect on the adsorption dynamic of methane molecules on shale powders. Obviously, it is shown that the adsorption rate constants all slowly drop with the equilibrium pressure increasing under different temperature conditions, revealing that it is much easier for methane molecules to adsorb on gas shale powders at a higher pressure. This is mainly because at a higher pressure condition, the high concentration driving force is the main controlling force that can promote the adsorption rate of methane molecules. Moreover, at the same pressure point, a smaller Bangham adsorption rate constant is attained due to a higher temperature, which indicates low temperatures are favorable for methane adsorption on shale powders. This is mainly because the methane adsorption dynamic on shale powders is exothermic.

Furthermore, to quantitatively analyze the relationship between the adsorption rate constant and the equilibrium pressure, the linear correlation relationships between k (adsorption rate constant) and $\ln(P)$ at 30, 40 and 50 °C are plotted in a semi-logarithmic coordinate system, as shown in Figure 10. The fitted results are, respectively, expressed as follows:

$$30\text{ }^{\circ}\text{C} \quad k = 0.6973\ln(P) + 1.2983 \quad R^2 = 0.9932 \quad (7)$$

$$40\text{ }^{\circ}\text{C} \quad k = 0.7583\ln(P) + 0.9269 \quad R^2 = 0.9924 \quad (8)$$

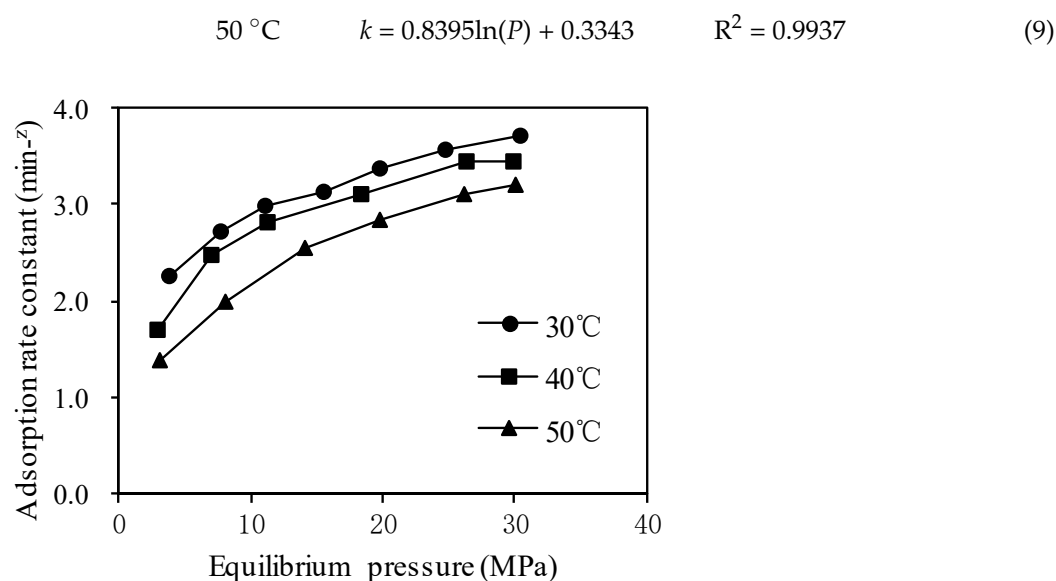


Figure 9. Adsorption rate constant versus equilibrium pressure at different temperature.

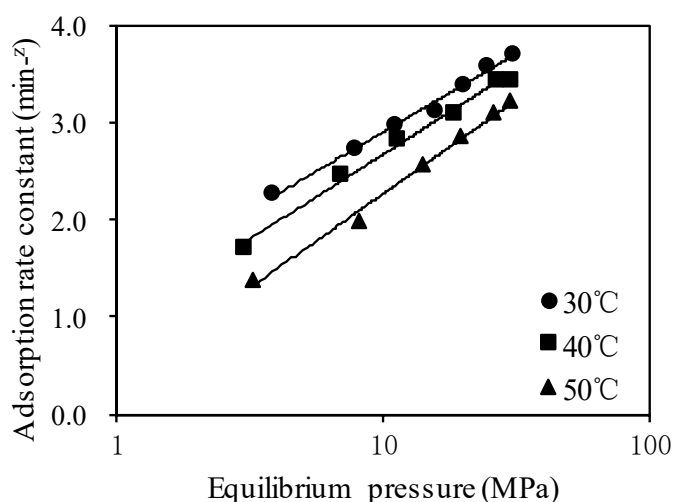


Figure 10. The relationship between adsorption rate constant and equilibrium pressure.

The correlation coefficients at 30, 40 and 50 °C, respectively, are 0.9932, 0.9924 and 0.9937, indicating that the adsorption rate constant is linearly positively correlated with the natural log of the equilibrium pressure.

4.5. Effect of Temperature on Adsorption Isotherm

To compare the difference in the adsorption amount at different temperatures, the adsorption amounts under different equilibrium pressures at 30, 40 and 50 °C are plotted versus the equilibrium pressure in Figure 11. It is clearly shown that the adsorption amount under the different equilibrium pressure at 30 °C is the biggest, followed by that of 40 °C and 50 °C, which indicates low temperatures are favorable for methane adsorption on shale powders. Figure 12 shows the plot of adsorption amount versus equilibrium pressure in a logarithmic coordinate system at each stable temperature. Obviously, it is shown that the adsorption amount is linearly positively correlated with the equilibrium pressure. The fitted results, including the fitted equation, the correlation coefficient (R^2), the Freundlich model, the Freundlich constant K and the constant n , are listed in Table 4. The correlation coefficients at 30, 40 or 50 °C, respectively, are 0.9945, 0.9987 and 0.9925, indicating that the relationship between the adsorption amount and the equilibrium pressure can be well fitted by the Freundlich model. K (Freundlich constant) at 30, 40 and 50 °C, respectively, is

5.1487, 2.1062 and 1.7857, indicating that K decreases with the temperature increasing. The constant n , respectively, is 0.2182, 0.2120 and 0.1967, revealing that the constant n decreases with the temperature increasing. Therefore, low temperatures are favorable for methane adsorption on shale powders, and high temperatures can obviously reduce constant K and n of the Freundlich model.

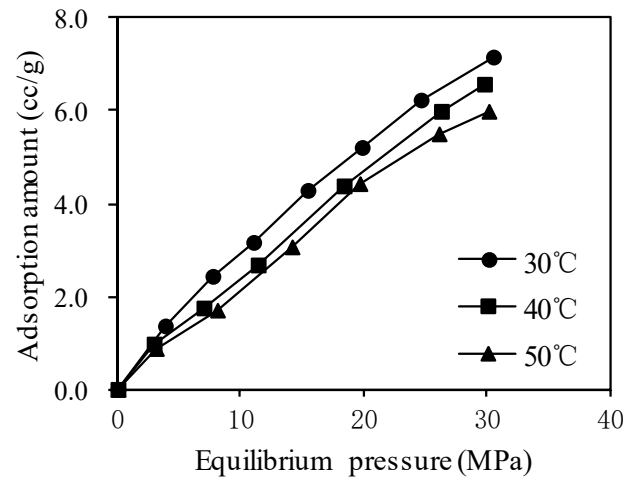


Figure 11. Adsorption amount versus equilibrium pressure at different temperature.

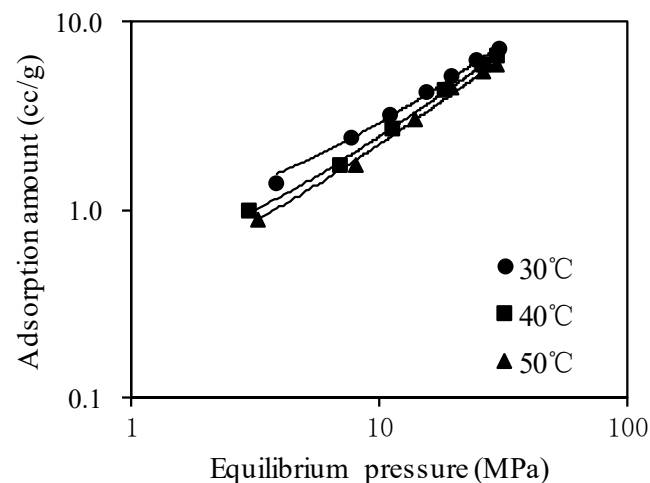


Figure 12. The relationship between adsorption amount and equilibrium pressure.

Table 4. The results of fitting methane adsorption isotherm at different temperatures.

NO	T (°C)	Fitting Equation	R ²	Freundlich Model	K	n
1	30	$y = 0.2182x + 0.7117$	0.9945	$V = 5.1484P^{0.2182}$	5.1487	0.2182
2	40	$y = 0.2120x + 0.3235$	0.9987	$V = 2.1062P^{0.2120}$	2.1062	0.2120
3	50	$y = 0.1967x + 0.2518$	0.9925	$V = 1.7857P^{0.1967}$	1.7857	0.1967

4.6. Effect of Temperature on Isostatic Enthalpy

The isostatic enthalpy of methane adsorption is derived from the Van't Hoff equation, and it is expressed as follows [16]:

$$\left(\frac{\partial \ln P}{\partial T}\right)_n = \frac{\Delta H}{RT^2} \quad (10)$$

where P is the pressure in kPa, T is the temperature in K, n is the absolute adsorption amount, R is the ideal gas constant in kJ/mol, and ΔH is the enthalpy of adsorption in kJ/mol.

Equation (10) can be integrated and rearranged, and the linear form of this model can be expressed as

$$\ln P = a \frac{1}{T} + b \tag{11}$$

where $a = -\frac{\Delta H}{R}$, $b = \frac{\Delta H}{R} \frac{1}{T_0} + \ln P_0$. The plot of $\ln P$ versus $1/T$ should be fitted as a linear equation, and then, ΔH can be calculated according to the slope of a .

Figure 13 shows the plot of $\ln P$ versus n (adsorption amount) at 30, 40 or 50 °C. The fitted results, including the temperature, the fitting equation, the correlation coefficient (R^2) and the parameters of the fitted equation, are listed in Table 5. It is clearly shown that there exists a well-linear relationship between $\ln P$ and n because the correlation coefficients, respectively, are 0.9471, 0.9142 and 0.9205, with the average of 0.9273. The slopes of the fitted equation increase with the temperature increasing. Moreover, by using the fitted equation listed in Table 5, the values of $\ln P$ at different temperatures are calculated and shown in Table 6.

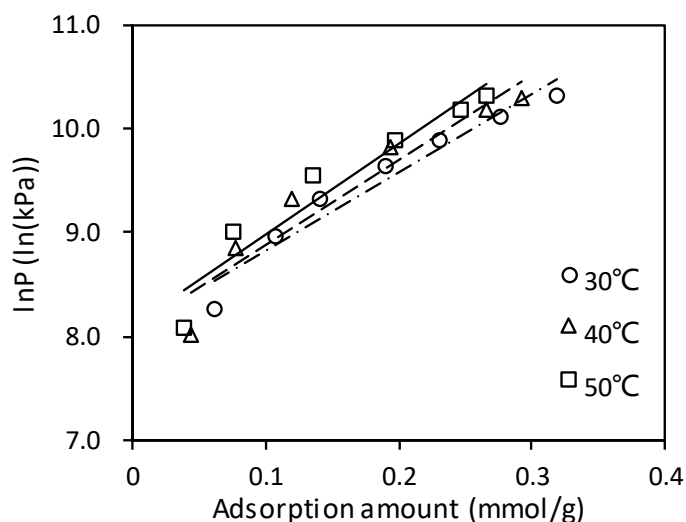


Figure 13. The relationship between $\ln P$ and n .

Table 5. Fitting results of $\ln P$ and n at different temperatures.

T (°C)	Fitting Equation	R^2	Slop	y-Intercept
30	$y = 7.5569x + 8.0708$	0.9471	7.5569	8.0708
40	$y = 8.2189x + 8.0551$	0.9142	8.2189	8.0551
50	$y = 8.7860x + 8.0984$	0.9205	8.7860	8.0984

Table 6. Calculation results of $\ln P$ at different temperatures.

n (mmol/g)	$\ln P$		
	30 °C	40 °C	50 °C
0.05	8.45	8.47	8.54
0.10	8.83	8.88	8.98
0.15	9.20	9.29	9.42
0.20	9.58	9.70	9.86
0.25	9.96	10.11	10.29
0.30	10.34	10.52	10.73
0.35	10.72	10.93	11.17

The relationship of $\ln P$ and $1/T$ under different given adsorption amounts is shown in Figure 14, and the fitted results, including the adsorption amount, the fitted equation, the correlation coefficient (R^2) and the parameters of the fitted equation, are listed in Table 7. It can be seen that $\ln P$ is linearly positively correlated with $1/T$ because R^2 is distributed between 0.8781 and 0.9974, with the average of 0.9705. Furthermore, isostatic enthalpy can be obtained, and the plot of isostatic enthalpy versus adsorption amount is shown in Figure 15. Obviously, it is shown that there exists a good linear relationship between isostatic enthalpy and the adsorption amount, indicating that isostatic enthalpy is linearly positively correlated with the adsorption amount.

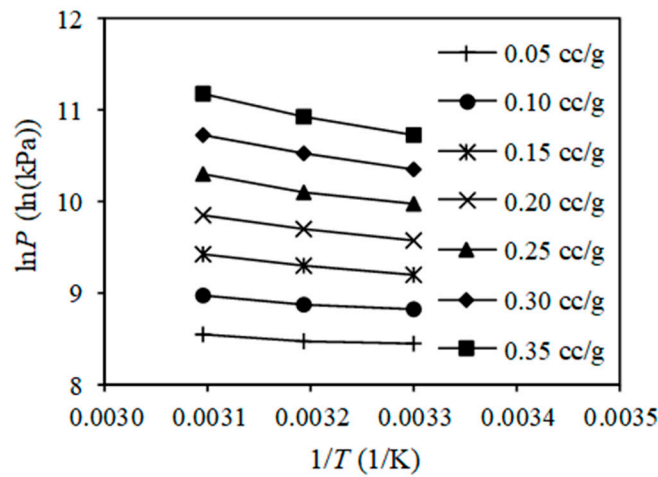


Figure 14. The relationship between $\ln P$ and $1/T$ under different given adsorption amount.

Table 7. The results of fitting $\ln P$ and $1/T$ under different given adsorption amount.

n (mmol/g)	Fitting Equation	R^2	a	b
0.05	$y = -433.23x + 9.87$	0.8781	-433.23	9.87
0.10	$y = -734.39x + 11.24$	0.9581	-734.39	11.24
0.15	$y = -1035.55x + 12.61$	0.9806	-1035.55	12.61
0.20	$y = -1336.71x + 13.98$	0.9895	-1336.71	13.98
0.25	$y = -1637.87x + 15.36$	0.9937	-1637.87	15.36
0.30	$y = -1939.03x + 16.73$	0.9961	-1939.03	16.73
0.35	$y = -2240.19x + 18.10$	0.9974	-2240.19	18.10

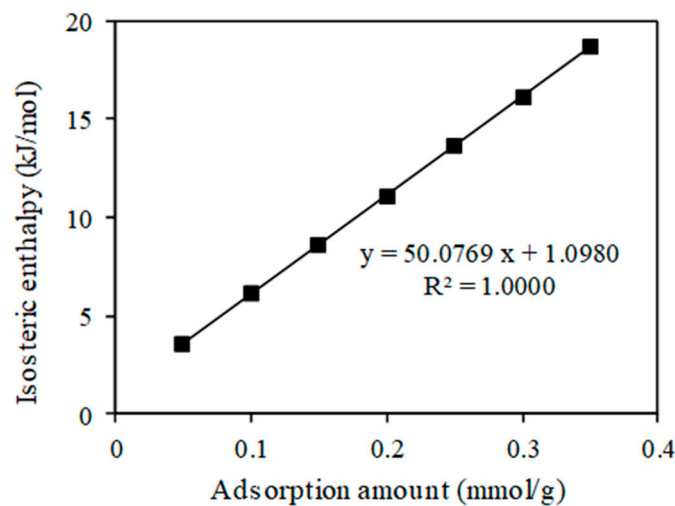


Figure 15. The relationship between isostatic enthalpy and adsorption amount.

5. Conclusions

The curves of the pressure response at different pressure steps and temperatures all have the same tendency to drop fast at first, then slowly in the middle and remain stable at last, and the adsorption amount increases quickly at first, then slowly in the middle and remains constant at last, revealing that the methane molecules are mainly adsorbed in the initial stage.

The adsorption amount (q_t) can be well fitted with time (t) by using the Bangham model at each pressure step. The constant z first decreases and then increases with the equilibrium pressure increasing at each temperature, and it decreases with the temperature increasing at the same pressure. The adsorption rate constant is linearly positively correlated with the natural log of the equilibrium pressure, and it decreases with the temperature increasing at the same pressure.

The Freundlich model can well fit the relationship between the adsorption amount and the equilibrium pressure. The constant K and n of the Freundlich model all decrease with the temperature increasing, indicating that the low temperature is favorable for methane adsorption on shale powders, and the high temperature can obviously reduce the constant K and n of the Freundlich model.

There exists a well-linear relationship between $\ln P$ and n at different temperatures. $\ln P$ is linearly positively correlated with $1/T$ under different given adsorption amounts. Isostatic enthalpy is linearly positively correlated with the adsorption amount.

Author Contributions: Conceptualization, H.Z. and Z.L.; methodology, Y.Z.; formal analysis, P.X.; data curation, A.H.; writing—original draft preparation, Y.Z.; writing—review and editing, Y.Z. and Z.L. All authors have read and agreed to the published version of the manuscript.

Funding: This research is supported by National Key Research and Development Program of China, grant number Sinopec Huabei Sub-Company Subcontract No. 2017ZX05049, and the Scientific and Technological Research Program of Chongqing Municipal Education Commission, grant number KJQN202101502.

Institutional Review Board Statement: Not applicable.

Informed Consent Statement: Not applicable.

Data Availability Statement: The data that support the findings of this study are available from the corresponding author upon reasonable request.

Conflicts of Interest: The authors declare no conflict of interest.

References

1. Ross, D.J.K.; Marc Bustin, R. Impact of mass balance calculations on adsorption capacities in microporous shale gas reservoirs. *Fuel* **2007**, *86*, 2696–2706. [[CrossRef](#)]
2. Curtis, J.B. Fractured shale-gas systems. *Am. Assoc. Pet. Geol. Bull.* **2002**, *86*, 1921–1938.
3. Wang, J.; Dong, M.; Yang, Z.; Gong, H.; Li, Y. Investigation of methane desorption and its effect on the gas production process from shale: Experimental and mathematical study. *Energy Fuels* **2017**, *31*, 205–216. [[CrossRef](#)]
4. Pan, Z.; Connell, L.D. Reservoir simulation of free and adsorbed gas production from shale. *J. Nat. Gas Sci. Eng.* **2015**, *22*, 359–370. [[CrossRef](#)]
5. Wang, J.; Wang, B.; Li, Y.; Yang, Z.; Gong, H.; Dong, M. Measurement of dynamic adsorption-diffusion process of methane in shale. *Fuel* **2016**, *172*, 37–48. [[CrossRef](#)]
6. Wu, F.C.; Tseng, R.L.; Juang, R.S. Initial behavior of intraparticle diffusion model used in the description of adsorption kinetics. *Chem. Eng. J.* **2009**, *153*, 1–8. [[CrossRef](#)]
7. Guo, C.; Li, R.; Sun, J.; Wang, X.; Liu, H. A review of gas transport and adsorption mechanisms in two-component methane-carbon dioxide system. *Int. J. Energy Res.* **2020**, *44*, 2499–2516. [[CrossRef](#)]
8. Dasani, D.; Wang, Y.; Tsotsis, T.T.; Jessen, K. Laboratory-Scale Investigation of Sorption Kinetics of Methane/Ethane Mixtures in Shale. *Ind. Eng. Chem. Res.* **2017**, *56*, 9953–9963. [[CrossRef](#)]
9. Chalmers, G.R.L.; Bustin, R.M. Lower Cretaceous gas shales in northeastern British Columbia, Part I: Geological controls on methane sorption capacity. *Bull. Can. Pet. Geol.* **2008**, *56*, 22–61. [[CrossRef](#)]

10. Manger, K.C.; Oliver, S.J.P.; Curtis, J.B.; Scheper, R.J. Geologic influences on the location and production of Antrim Shale gas, Michigan Basin. In Proceedings of the Rocky Mountain Regional/Low Permeability Reservoirs Symposium and Exhibition Rocky Mountain Regional/Low Permeability Reservoirs Symposium and Exhibition, Denver, CO, USA, 15–17 April 1991.
11. Heller, R.; Zoback, M. Adsorption of methane and carbon dioxide on gas shale and pure mineral samples. *J. Unconv. Oil Gas Resour.* **2014**, *8*, 14–24. [[CrossRef](#)]
12. Chen, J.; Wang, F.C.; Liu, H.; Wu, H.A. Molecular mechanism of adsorption/desorption hysteresis: Dynamics of shale gas in nanopores. *Sci. China Physics, Mech. Astron.* **2017**, *60*, 014611. [[CrossRef](#)]
13. Ross, D.J.K.; Marc Bustin, R. The importance of shale composition and pore structure upon gas storage potential of shale gas reservoirs. *Mar. Pet. Geol.* **2009**, *26*, 916–927. [[CrossRef](#)]
14. Zhang, T.; Ellis, G.S.; Ruppel, S.C.; Milliken, K.; Yang, R. Effect of organic-matter type and thermal maturity on methane adsorption in shale-gas systems. *Org. Geochem.* **2012**, *47*, 120–131. [[CrossRef](#)]
15. Fan, K.; Li, Y.; Elsworth, D.; Dong, M.; Yin, C.; Li, Y.; Chen, Z. Three stages of methane adsorption capacity affected by moisture content. *Fuel* **2018**, *231*, 352–360. [[CrossRef](#)]
16. Rexer, T.F.T.; Benham, M.J.; Aplin, A.C.; Thomas, K.M. Methane adsorption on shale under simulated geological temperature and pressure conditions. *Energy Fuels* **2013**, *27*, 3099–3109. [[CrossRef](#)]
17. Hu, A.; Zhang, Y.; Xiong, P.; Yang, Y.; Liu, Z. Kinetic characteristics and modeling comparison of methane adsorption on gas shale. *Energy Sources Part A Recover. Util. Environ. Eff.* **2020**, *00*, 1–15. [[CrossRef](#)]
18. Liu, Z.; Bai, B.; Wang, Y.; Ding, Z.; Li, J.; Qu, H.; Jia, Z. Experimental study of friction reducer effect on dynamic and isotherm of methane desorption on Longmaxi shale. *Fuel* **2021**, *288*, 119733. [[CrossRef](#)]
19. Meng, M.; Zhong, R.; Wei, Z. Prediction of methane adsorption in shale: Classical models and machine learning based models. *Fuel* **2020**, *278*, 118358. [[CrossRef](#)]
20. Plazinski, W.; Dziuba, J.; Rudzinski, W. Modeling of sorption kinetics: The pseudo-second order equation and the sorbate intraparticle diffusivity. *Adsorption* **2013**, *19*, 1055–1064. [[CrossRef](#)]
21. Guo, C.; Li, R.; Wang, X.; Liu, H. Study on two component gas transport in nanopores for enhanced shale gas recovery by using carbon dioxide injection. *Energies* **2020**, *13*, 1101. [[CrossRef](#)]
22. Wu, K.; Li, X.; Wang, C.; Yu, W.; Chen, Z. Model for surface diffusion of adsorbed gas in nanopores of shale gas reservoirs. *Ind. Eng. Chem. Res.* **2015**, *54*, 3225–3236. [[CrossRef](#)]
23. Yuan, W.; Pan, Z.; Li, X.; Yang, Y.; Zhao, C.; Connell, L.D.; Li, S.; He, J. Experimental study and modelling of methane adsorption and diffusion in shale. *Fuel* **2014**, *117*, 509–519. [[CrossRef](#)]
24. Chen, L.; Zuo, L.; Jiang, Z.; Jiang, S.; Liu, K.; Tan, J.; Zhang, L. Mechanisms of shale gas adsorption: Evidence from thermodynamics and kinetics study of methane adsorption on shale. *Chem. Eng. J.* **2019**, *361*, 559–570. [[CrossRef](#)]
25. Rani, S.; Prusty, B.K.; Pal, S.K. Adsorption kinetics and diffusion modeling of CH₄ and CO₂ in Indian shales. *Fuel* **2018**, *216*, 61–70. [[CrossRef](#)]
26. Yang, Z.; Wang, W.; Dong, M.; Wang, J.; Li, Y.; Gong, H.; Sang, Q. A model of dynamic adsorption-diffusion for modeling gas transport and storage in shale. *Fuel* **2016**, *173*, 115–128. [[CrossRef](#)]
27. Reveles, R.; Bangham, M.; Allen, J.; Schwartz, J.; Lambert, R.; Mangan, B. Characteristics of methane-oxygen combustion in explosions. In Proceedings of the 2018 Joint Propulsion Conference, Cincinnati, OH, USA, 9–11 July 2018.
28. Wang, Y.; Zhu, Y.; Liu, S.; Zhang, R. Methane adsorption measurements and modeling for organic-rich marine shale samples. *Fuel* **2016**, *172*, 301–309. [[CrossRef](#)]
29. Guo, J.; Zhai, Z.; Wang, L.; Wang, Z.; Wu, J.; Zhang, B.; Zhang, J. Dynamic and thermodynamic mechanisms of TFA adsorption by particulate matter. *Environ. Pollut.* **2017**, *225*, 175–183. [[CrossRef](#)]
30. Dada, A.O.; Olalekan, A.P.; Olatunya, A.M.; Dada, O.J. Langmuir, Freundlich, Temkin and Dubinin—Radushkevich Isotherms Studies of Equilibrium Sorption of Zn²⁺ Unto Phosphoric Acid Modified Rice Husk. *IOSR J. Appl. Chem.* **2012**, *3*, 38–45. [[CrossRef](#)]
31. Kanô, F.; Abe, I.; Kamaya, H.; Ueda, I. Fractal model for adsorption on activated carbon surfaces: Langmuir and Freundlich adsorption. *Surf. Sci.* **2000**, *467*, 131–138. [[CrossRef](#)]
32. Umpleby, R.J.; Baxter, S.C.; Bode, M.; Berch, J.K.; Shah, R.N.; Shimizu, K.D. Application of the Freundlich adsorption isotherm in the characterization of molecularly imprinted polymers. *Anal. Chim. Acta* **2001**, *435*, 35–42. [[CrossRef](#)]
33. Zhang, L.; Li, J.; Jia, D.; Zhao, Y.; Xie, C.; Tao, Z. Study on the adsorption phenomenon in shale with the combination of molecular dynamic simulation and fractal analysis. *Fractals* **2018**, *26*, 1–15. [[CrossRef](#)]
34. Zhou, S.; Xue, H.; Ning, Y.; Guo, W.; Zhang, Q. Experimental study of supercritical methane adsorption in Longmaxi shale: Insights into the density of adsorbed methane. *Fuel* **2018**, *211*, 140–148. [[CrossRef](#)]
35. Mall, I.D.; Srivastava, V.C.; Agarwal, N.K. Removal of Orange-G and Methyl Violet dyes by adsorption onto bagasse fly ash—Kinetic study and equilibrium isotherm analyses. *Dye. Pigment.* **2006**, *69*, 210–223. [[CrossRef](#)]